

Ultrastrong coupling in a scalable design for circuit QED with superconducting flux qubits

Mun Dae Kim

Received: date / Accepted: date

Abstract We theoretically study a circuit quantum electrodynamics (QED) architecture with superconducting flux qubits. The qubit is coupled to the transmission line resonator by an ac current originating from the current mode of the resonator. Ultrastrong coupling can be obtained by varying the capacitance between the qubit and the resonator. We propose a scalable design where the two-qubit coupling can be achieved.

Keywords circuit quantum electrodynamics · flux qubit · ultrastrong coupling · scalable design

1 Introduction

An artificial two level system can be coupled with the quantized electromagnetic field in a superconducting transmission line resonator, while a natural atom is coupled with cavity. This circuit quantum electrodynamics (QED) architecture [1,2] is a solid-state analog of cavity QED, providing a strong coupling strength between the qubit and resonator owing to the large dipole moment of the artificial qubit. The circuit QED scheme has been applied to superconducting qubits among which the flux qubit [3,4,5] has the advantage of fast gate operation because the flux qubit does not require low anharmonicity for long coherence time. There have been many studies for the circuit QED with the superconducting flux qubit [6,7]. However, the inductive coupling between the flux qubit and the transmission line resonator of the circuit is too weak to perform the quantum gate operation.

Recently a galvanic coupling scheme for the circuit QED with the flux qubits has been proposed to enhance the coupling strength by sharing the flux qubit loop with the resonator transmission line [8,9,10]. On the other

Mun Dae Kim
Korea Institute for Advanced Study, Seoul 130-722, Korea
E-mail: mdkim@kias.re.kr

hand, for the scheme with ac current coupling between the flux qubit and the transmission line resonator [11,12,13,14], the qubit and the resonator are not galvanically coupled with each other, but by a ac current flowing through the capacitance between the qubit and the resonator. In this scheme the three-junctions flux qubit is coupled by ac current, similarly to the superconducting phase qubit [15,16,17,18]. While the states of phase qubit are defined in terms of the phase degrees of freedom in a washboard type potential, the present flux qubit uses the persistent current states as qubit states. The qubit state preparation and the quantum gate operation are achieved by the ac current. Indeed, the present flux qubit thus has the advantages of phase qubit such as fast qubit operation and readout, individual addressing, and scalability.

This ac current coupling has recently been implemented in experiments where three-junctions flux qubit is located at the end of the resonator [12,13,14]. In this study, we introduce a scalable design where qubits are located at the nodes of the resonator current mode so that many qubits can be controlled by using a higher harmonic mode of resonator current. We propose a qubit scheme which can provide ultrastrong coupling. The ultrastrong coupling can perform numerous quantum optics effects in solid state device [10,19] and provide a long coherence time [20] in addition to a fast qubit operation [21]. In the qubit scheme the capacitance between the qubit and the resonator can be controlled by varying the width of capacitance line, extended from the qubit loop, and the distance between the capacitance line and the transmission line resonator. In the scalable design the qubit-resonator coupling depends on the number of qubits in the circuit. By varying number of qubits we calculate the qubit-resonator coupling which shows a maximum of ultrastrong coupling with reasonable parameter values. Further we analyze the xy-type interaction between two qubits which can also reach ultrastrong coupling regime.

2 Circuit-QED with superconducting flux qubits

Usually the transmon qubit is coupled with the voltage mode of the transmission line resonator through a capacitance [1,2,22]. For superconducting flux qubits, there have been many studies to couple the flux qubit with the current mode of the transmission line resonator by using mutual inductance between the qubit loop and the resonator [6,7] or by sharing the qubit loop with the resonator [8,9,10]. On the other hand the three-junctions flux qubit can also be coupled with the transmission line resonator through a capacitance, but in this case it is coupled with the ac current from the resonator. Ac current flowing across the capacitance gives rise to the coupling between the qubit and the resonator [11,12,13,14].

We consider a qubit design shown in Fig. 1(a), where the three-junctions flux qubits are located at the nodes of the current mode of the resonator. In this scalable design the qubits are coupled with the transmission line resonator by a capacitance line extended from the qubit loop. The width w of the capacitance line and the distance d between the capacitance line and the resonator can be

adjusted to determine the capacitance between the qubit and the resonator. Two capacitors at the ends of the resonator are introduced for the current mode of the resonator to be periodic in a scalable design.

The microwave passing through the uniform resonator in the circuit QED architecture can be described as a one-dimensional motion by the Lagrangian

$$\mathcal{L}(\theta, \dot{\theta}; t) = \int_{-L/2}^{L/2} \left(\frac{l}{2} (\dot{\theta}(x, t))^2 - \frac{1}{2c} (\nabla \theta(x, t))^2 \right) dx, \quad (1)$$

where l and c are the inductance and the capacitance per unit length of the uniform transmission line resonator, respectively, and $\theta(x, t) = \int_{-L/2}^x dx' q(x', t)$ with the linear charge density $q(x)$ is a collective field variable. In the present design the resonator is not uniform any more. We thus start with the equation of motion of the field variable in the sector k of the resonator given by the Euler-Lagrange equation

$$\frac{1}{c_k} \frac{\partial^2 \theta_k(x, t)}{\partial x^2} - l \frac{\partial^2 \theta_k(x, t)}{\partial t^2} = 0 \quad (2)$$

with the capacitance density c_k of sector k .

By representing the field variable as a product of spatial and temporal parts $\theta_k(x, t) = X_k(x)\phi(t)$, we get the equation for the spatial part wavefunction $(1/c_k)(\partial^2/\partial x^2)X_k(x) + l\omega_r^2 X_k(x) = 0$. From this equation we can readily

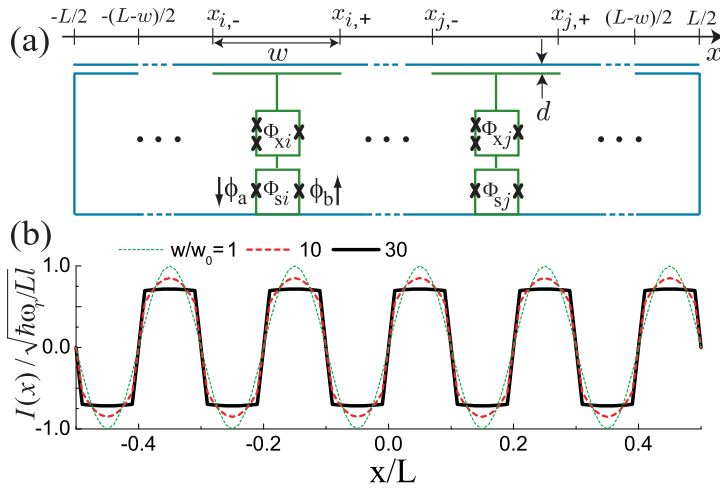


Fig. 1 (a) A schematic diagram for a scalable design of circuit QED with superconducting three-junctions flux qubits. Here we show, for example, two qubits. The dc-SQUIDS between qubit and ground plane plays the role of switching the coupling between qubit and resonator. The capacitance line has the width of w and the distance between the capacitance line and the resonator is d . (b) Current profiles when there are nine qubits in the circuit of (a) for $(d_0/d, w/w_0) = (1, 1), (5, 10), (15, 30)$. Nine current jumps appear at qubit sites, and grow as the width w of capacitance line increases.

observe that $(1/c_k)\partial X_k(x)/\partial x$ and $X_k(x)$ are continuous at the boundary between the sectors, which means the continuity of electric potential $V_k(x, t) = (1/c_k)\partial\theta(x, t)/\partial x = (1/c_k)\nabla X_k(x)\phi(t)$ and current $I(x, t) = \partial\theta(x, t)/\partial t = X(x)\dot{\phi}(t)$ at the boundaries.

Let's consider the case that the number of qubit N is odd. Then the spatial part $X(x)$ ($-N-1 \leq k \leq N+1$) of the wavefunction is written as

$$X(x) = \begin{cases} A_{-N-1}e^{i\frac{j_2\pi}{L}x} + B_{-N-1}e^{-i\frac{j_2\pi}{L}x} & (-\frac{L}{2} < x < -\frac{L}{2} + \frac{w}{2}) \\ \vdots & \\ A_{k_o}e^{i\frac{j_1\pi}{L}x} + B_{k_o}e^{-i\frac{j_1\pi}{L}x} & (x_{k_o-1,+} < x < x_{k_o+1,-}) \\ \vdots & \\ A_{k_e}e^{i\frac{j_2\pi}{L}x} + B_{k_e}e^{-i\frac{j_2\pi}{L}x} & (x_{k_e-} < x < x_{k_e+}) \\ \vdots & \\ A_{N+1}e^{i\frac{j_2\pi}{L}x} + B_{N+1}e^{-i\frac{j_2\pi}{L}x} & (\frac{L}{2} - \frac{w}{2} < x < \frac{L}{2}), \end{cases} \quad (3)$$

where $x_{k\pm} = \frac{k}{N+1}\frac{L}{2} \pm \frac{w}{2}$, $x_{-N-1,-} = -\frac{L}{2}$, and $x_{N+1,+} = \frac{L}{2}$ with k_e (k_o) being even (odd) integer among $k = 0, \pm 1, \pm 2, \dots, \pm(N+1)$. The capacitance line covers the range $x_{k_e-} < x < x_{k_e+}$ where a qubit is located. In this region we set $c_k = c'$ and $j_k = j_2$. Otherwise, we set $c_k = c$ and $j_k = j_1$ in the region $x_{k_o-1,+} < x < x_{k_o+1,-}$ where there is no qubit [see, for example, Fig. 2]. From the equation for $X_k(x)$ we obtain

$$\frac{1}{\sqrt{lc}} \frac{j_1\pi}{L} = \frac{1}{\sqrt{lc'}} \frac{j_2\pi}{L} = \omega_r. \quad (4)$$

The conditions for continuity of $X(x)$ at, for example, $x = x_{k_o-1,+}$ and $x = x_{k_e-}$ are given by

$$A_{k_o-1}e^{i\frac{j_2\pi}{L}x_{k_o-1,+}} + B_{k_o-1}e^{-i\frac{j_2\pi}{L}x_{k_o-1,+}} = A_{k_o}e^{i\frac{j_1\pi}{L}x_{k_o-1,+}} + B_{k_o}e^{-i\frac{j_1\pi}{L}x_{k_o-1,+}}, \quad (5)$$

$$A_{k_e-1}e^{i\frac{j_1\pi}{L}x_{k_e-}} + B_{k_e-1}e^{-i\frac{j_1\pi}{L}x_{k_e-}} = A_{k_e}e^{i\frac{j_2\pi}{L}x_{k_e-}} + B_{k_e}e^{-i\frac{j_2\pi}{L}x_{k_e-}} \quad (6)$$

with $k = 0, \pm 1, \pm 2, \dots, \pm N, N+1$, respectively, and the boundary conditions at both ends of resonator are

$$A_{-N-1}e^{-i\frac{j_2\pi}{2}} + B_{-N-1}e^{i\frac{j_2\pi}{2}} = 0, \quad (7)$$

$$A_{N+1}e^{i\frac{j_2\pi}{2}} + B_{N+1}e^{-i\frac{j_2\pi}{2}} = 0. \quad (8)$$

From the condition for continuity of $(1/c_k)dX_k(x)/dx$ similar equations are also obtained.

In order to categorize the boundary conditions into even parity and odd parity parts we set $k_e = -k_o + 1$ and use the relation $x_{-k_e,o,\pm} = -x_{k_e,o,\mp}$ to represent, for example, Eq. (5) in terms of k_e and Eq. (6) in terms of k_o . Then, all boundary conditions can be transformed into two sets with the variables of either (i) $A_{-k} + B_k$ or (ii) $A_{-k} - B_k$. Each set can be treated as an independent eigenvalue problem. If the determinant of the matrix corresponding to set (i)

is non-zero while that for (ii) is zero, we have an odd parity solution such as $A_{-k} = -B_k$. Around the central qubit site the solution becomes $X_0(x) \sim A_0 \sin \frac{j_2 \pi}{L} x$. On the contrary, if the determinant for (i) is zero while that for (ii) is non-zero, we have an even parity solution such as $A_{-k} = B_k$ and thus $X_0(x) \sim A_0 \cos \frac{j_2 \pi}{L} x$. For the case that the number of qubits N is even, a similar analysis can also be performed.

The Lagrangian in Eq. (19) of the resonator modes can be written as $\mathcal{L}(\phi, \dot{\phi}) = L \left(\frac{1}{2} \mu \dot{\phi}^2 - \frac{1}{2c} \kappa \phi^2 \right)$ with dimensionless constant $\mu = (1/L) \sum_k \int_{-L/2}^{L/2} X_k^2(x) dx$ and $\kappa = (1/L) \sum_k \int_{-L/2}^{L/2} (c/c_k) (\nabla X_k(x))^2 dx$. If we introduce the representations

$$\dot{\phi}(t) = \frac{-i}{\sqrt{2\mu}} \sqrt{\frac{\hbar\omega_r}{Ll}} (a - a^\dagger), \quad (9)$$

$$\phi(t) = \frac{1}{\sqrt{2\kappa}} \sqrt{\frac{\hbar\omega_r c}{L}} (a + a^\dagger), \quad (10)$$

the Hamiltonian of the resonator modes is written in a diagonalized form $H_r = \hbar\omega_r (a^\dagger a + \frac{1}{2})$. The current $I(x, t) = X(x)\dot{\phi}(t)$ is then given by

$$I(x, t) = -i \frac{X(x)}{\sqrt{2\mu}} \sqrt{\frac{\hbar\omega_r}{Ll}} (a - a^\dagger). \quad (11)$$

In Fig. 1(b) we show the resonator current profiles for 9 qubits, which is calculated numerically by using 10th harmonic mode of the resonator current. In the figure we can observe current jumps at the nodes of the current profile

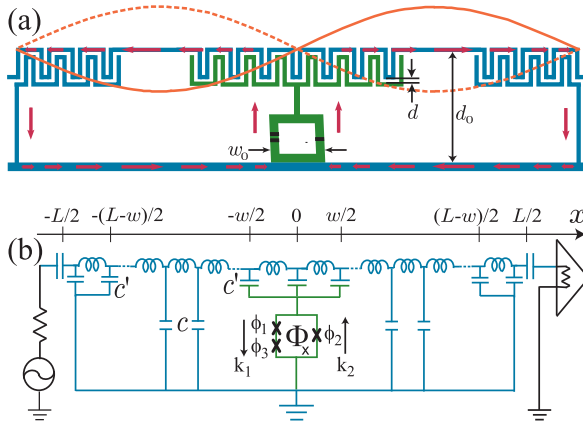


Fig. 2 (a) A superconducting three-junctions flux qubit where w_0 is the width of qubit loop and d_0 the distance between the resonator and the ground plane. The upper superconducting plane is the transmission line resonator and the lower is the ground plane. The arrows show the current in the circuit corresponding to the second harmonic current mode. (b) The schematic diagram for the circuit in (a), where c and c' are the capacitance density between the resonator and the ground plane and between the resonator and the qubit, respectively. The three Josephson junctions with phase difference ϕ_i are located asymmetrically.

where qubits are located. These jumps increase along with w/w_0 and d_0/d with w_0 and d_0 denoted in Fig. 2 (a). The qubit-resonator coupling strength depends on the current jump as will be seen in the following.

For a single qubit case we can solve the problem analytically. In Fig. 2(a) the qubit is located at the node of the second harmonic mode of the resonator current. The resonator and the qubit are coupled by an ac current flowing into the qubit through the capacitance in the region $-w/2 < x < w/2$. The ac current is given by

$$I_b(t) = \int_{-w/2}^{w/2} \dot{q}(x, t) dx = I\left(\frac{w}{2}, t\right) - I\left(-\frac{w}{2}, t\right) \quad (12)$$

from the current conservation condition $\dot{q}(x, t) = \partial I(x, t)/\partial x$ in the resonator. Beyond the region $-w/2 < x < w/2$ ac current flows from the resonator to the ground plane directly through the capacitors with small capacitance density c in Fig. 2(b). The amplitude of ac current in Eq. (12) is given by

$$I_0 = \sqrt{\frac{\hbar\omega_r}{Ll}} \delta \quad \text{with} \quad \delta = 2 \frac{X(\frac{w}{2})}{\sqrt{2\mu}}, \quad (13)$$

where δ corresponds to the current jump in Figs. 1 and 3. Since the amplitude of current $I(x, t)$ in Eq. (11) satisfies the condition, $(1/L) \sum_k \int_{-L/2}^{L/2} (X_k(x)/\sqrt{2\mu})^2 dx = 0.5$, δ has the maximum value of $\sqrt{2}$ when the current profile takes the rectangular function form.

In Fig. 1(a) dc-SQUIDs are inserted between the qubit and the ground plane for switching on/off the qubit-resonator coupling. Φ_{xk} and Φ_{sk} are the external and switching flux for k -th qubit, respectively. The present flux qubit is coupled with the resonator through the ac current flowing across the capacitance between the qubit and the resonator. Hence, if we switch off the ac current by piercing a half-flux quantum into the dc-SQUID loop, the qubit and the resonator can be decoupled from each other. If the self inductance and the Josephson junction energy of the dc-SQUID loop is as small as those of the flux qubit, we have the boundary condition $\phi_a + \phi_b - 2\pi\Phi_{si}/\Phi_0 \approx 0$ for i -th dc-SQUID, where ϕ_a and ϕ_b are the phase differences across the Josephson junctions in the dc-SQUID. Then the total Josephson junction energy is written as $E_{JJ} = -E_{J,\text{eff}}(\Phi_{si}) \cos[(\phi_a - \phi_b)/2]$ with $E_{J,\text{eff}}(\Phi_{si}) = 2E_J \cos[(\phi_a + \phi_b)/2] = 2E_J \cos(\pi\Phi_{si}/\Phi_0)$, and the current flow can be blocked for the switching flux $\Phi_{si} = \Phi_0/2$ because $E_{J,\text{eff}}(\Phi_0/2) = 0$. This can be understood in another way: the effective Josephson inductance of the dc-SQUID, $L_J = (\Phi_0/2\pi)^2/E_{J,\text{eff}}(\Phi_{si})$, becomes infinite for $\Phi_{si} = \Phi_0/2$. Therefore, there can be no current flowing through, and thus the qubit-resonator coupling is switched off.

However, the boundary condition $\phi_a + \phi_b - 2\pi\Phi_{si}/\Phi_0 \approx 0$ is just an approximation neglecting an induced flux. Including the induced flux due to the current flowing through the dc-SQUID loop, the boundary condition is replaced by $\phi_a + \phi_b - 2\pi f_t = 0$, where $f_t = (\Phi_{si} + L'_s I')/\Phi_0$ with the self inductance L'_s and the current I' of dc-SQUID loop [23]. For a sufficiently small

dc-SQUID loop the self inductance L'_s and thus the induced flux $\Phi_{\text{ind}} = L'_s I'$ are negligible. However, in general, since the effective Josephson coupling energy becomes $E_{J,\text{eff}}(\Phi_{si}) = 2E_J \cos[(\phi_a + \phi_b)/2] = 2E_J \cos[\pi(\Phi_{si} + L'_s I')/\Phi_0]$, the external flux should be adjusted as $\Phi_{si} = \Phi_0/2 - L'_s I'$ in order to switch off the interaction.

3 Ultrastrong qubit-resonator coupling

When the qubit is located at the center of the resonator, the spatial part $X(x)$ should be an odd function, because the ac current of Eq. (12) vanishes if $X(x)$ is an even function for $-w/2 < x < w/2$. In this case the determinant of matrix corresponding to set (ii) of boundary conditions in section 2 should be zero, resulting in

$$e^{\frac{ij_1\pi}{2}(1-\frac{2w}{L})} = \pm \frac{cj_2 \cos \frac{j_2\pi}{2} \frac{w}{L} - ic'j_1 \sin \frac{j_2\pi}{2} \frac{w}{L}}{cj_2 \cos \frac{j_2\pi}{2} \frac{w}{L} + ic'j_1 \sin \frac{j_2\pi}{2} \frac{w}{L}}. \quad (14)$$

The values of j_1 , j_2 and ω_r are determined from Eqs. (4) and (14). For uniform capacitance density $c' = c$, j_1 and j_2 are integers, but in general they are non-integer depending on the ratio c'/c .

The spatial part $X_k(x)$ ($-2 \leq k \leq 2$) can be obtained by solving the boundary conditions in section 2 for $N = 1$. The set (i) of boundary conditions in section 2 provides the relation $A_{-k} = -B_k$, and the coefficients A_k and B_k are determined from the set (ii) of boundary conditions as

$$B_2 = -e^{ij_2\pi} A_2, \quad (15)$$

$$A_1 = -\frac{1}{j_1} e^{\frac{ij_1\pi}{2}(j_2-j_1(1-\frac{w}{L}))} \left(-\frac{cj_2}{c'} \cos \frac{j_2\pi}{2} \frac{w}{L} + ij_1 \sin \frac{j_2\pi}{2} \frac{w}{L} \right) A_2, \quad (16)$$

$$B_1 = -\frac{1}{j_1} e^{\frac{ij_1\pi}{2}(j_2+j_1(1-\frac{w}{L}))} \left(\frac{cj_2}{c'} \cos \frac{j_2\pi}{2} \frac{w}{L} + ij_1 \sin \frac{j_2\pi}{2} \frac{w}{L} \right) A_2, \quad (17)$$

$$A_0 = \frac{c'j_1}{2cj_2 \cos \frac{j_2\pi}{2} \frac{w}{L}} \left(e^{i\frac{j_1\pi}{2} \frac{w}{L}} A_1 - e^{-i\frac{j_1\pi}{2} \frac{w}{L}} B_1 \right). \quad (18)$$

In Fig. 3 (a) we show the current profile $I(x) = \frac{X(x)}{\sqrt{2\mu}} \sqrt{\frac{\hbar\omega_r}{Ll}}$, where we set $w_0/L = 10^{-4}$ corresponding to $w_0 = 1\mu\text{m}$ when $L = 10\text{mm}$. In the spatial part wave function $X(x)$ for $N = 1$ the remaining coefficient A_2 is a common factor in the numerator and denominator of $I(x)$, and thus is cancelled out. A finite current jump develops around the qubit location at the center of the resonator. Here, for simplicity, we assume that the capacitance c' between the resonator and the capacitance line increases linearly along with w/w_0 and d_0/d such that $c' = (wd_0/w_0d)c$. When $c' \gg c$, almost all current flows through the qubit at the center and the capacitors at the ends of the resonator, while just a weak current flows directly to ground through the small capacitance density c . As a result, we can observe a sharp change of current in Fig. 3.

Fig. 3(b) shows the central part of current profile closed by a dotted ellipse in Fig. 3(a) for various w/w_0 with fixed d_0/d , demonstrating a larger jump for larger w/w_0 . At the boundary ($x = \pm w/2$), the electric potential $(1/c_k)\partial X_k(x)/\partial x$ is continuous. Fig. 3(c) shows the currents for various d_0/d with fixed w/w_0 , which shows the jump also grows along with d_0/d . These figures show that the current jump δ grows along with both w/w_0 and d_0/d , and finally saturates at $\sqrt{2}$.

The coupling strength between the resonator and the three-junction flux qubit is given in terms of the amplitude of the bias-current I_0 . If the three-junction flux qubit is penetrated by a magnetic flux of half flux quantum $\Phi_0/2$, there are two current states in the qubit loop. The clockwise and counterclockwise current states correspond to the local minima in the effective potential of the qubit loop. Here we consider the usual Josephson junction energies such that $E_{J1} = 0.8E_{J2}$ and $E_{J2} = E_{J3}$ in the three-junction flux qubit of Fig. 2 [4,5,24]. In this case the phase difference α across the small Josephson junction can be obtained from Eq. (23) of Ref. [5] with $\lambda = E_{J1}/E_{J2} = 0.8$ and $\eta \approx E_L/E_{J2} = 50$ with E_L being the characteristic inductive energy, resulting in $\alpha \approx 0.38\pi$.

When a bias current I_b is applied to the flux qubit where three Josephson junctions are located asymmetrically in the loop as shown in Fig. 2, the

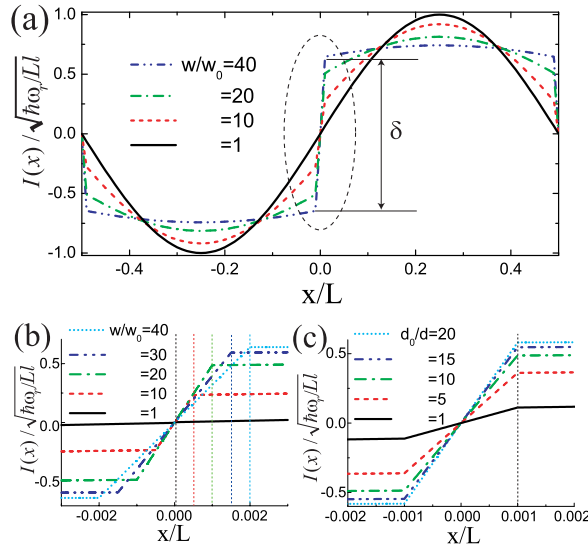


Fig. 3 (a) Current profile of single qubit case for various w/w_0 with $d_0/d = 10$ and $w_0/L = 10^{-4}$. The amount of jump δ around $x \approx 0$ increases along with w/w_0 . (b) The enlarged current profile around the jump inside the dotted ellipse in (a) for various w/w_0 with $d_0/d = 10$ and (c) for various d_0/d with $w/w_0 = 20$. Thin dotted lines indicate the boundary position $x = w/2$, the end of the capacitance line. As w/w_0 and d_0/d increase, the jump grows and finally saturates.

Lagrangian can be written as [11]

$$\mathcal{L}(\phi_i, \dot{\phi}_i) = \sum_{i=1}^3 \frac{1}{2} C_i \left(\frac{\Phi_0}{2\pi} \right)^2 \dot{\phi}_i^2 - U_{\text{eff}}(\{\phi_i\}), \quad (19)$$

$$U_{\text{eff}}(\{\phi_i\}) = \sum_{i=1}^3 E_{Ji} (1 - \cos \phi_i) + \frac{\Phi_0 I_b}{4\pi} (\phi_1 + \phi_3 - \phi_2) + \frac{\Phi_0^2}{2L_s} \left(n + f - \frac{1}{2\pi} \sum_{i=1}^3 \phi_i \right)^2, \quad (20)$$

where C_i is the capacitance of junction, L_s is the self inductance of the qubit loop, and $f = \Phi_x/\Phi_0$ with an external flux Φ_x threading the qubit loop and the superconducting unit flux quantum $\Phi_0 = h/2e$.

In the present circuit-QED scheme the current flowing into the qubit with width d is given by $I_b(t) = -iI_0[a(t) - a^\dagger(t)]$. Then the total Hamiltonian $H_{\text{JC}} = H_r + H_q + H_I$ given by the sum of the Hamiltonian for the resonator mode, for the qubit, and for the interaction between the resonator mode and the qubit is written as a Rabi type Hamiltonian [11]

$$\mathcal{H} = \hbar\omega_r a^\dagger a + \frac{\hbar\omega_a}{2} \sigma_z + ig\sigma_x(a - a^\dagger), \quad (21)$$

where ω_a is the qubit frequency and the last term represents the coupling between the qubit and the current mode in the resonator [11,14], which is

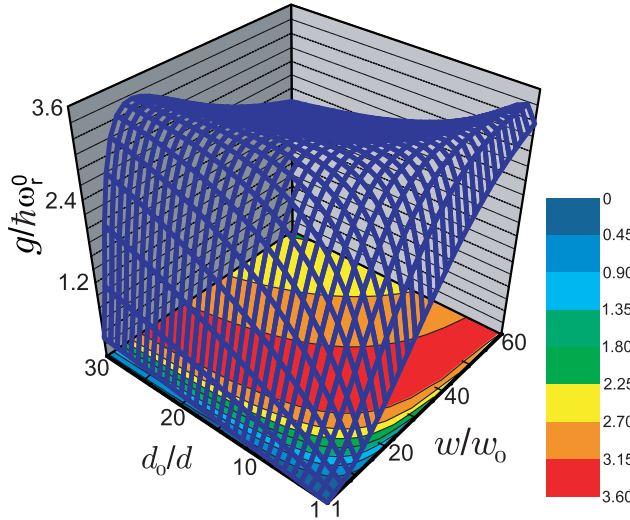


Fig. 4 Coupling constant g for the single qubit case in the plane of $(d_0/d, w/w_0)$ with the resonator impedance $Z = 50\Omega$. g has a maximum value corresponding to a ultrastrong coupling. At the bottom the contour plot of g is shown.

different from $g\sigma_x(a + a^\dagger)$ in the transmon case. The coupling strength g is given by a product of flux variable and bias current

$$g = \frac{\Phi_0}{2\pi} \alpha I_0 \quad (22)$$

similarly to the superconducting phase qubit [17, 25]. Here we have the phase difference α because the two phases in different sides of the qubit cancel each other out. Thus an asymmetrical layout of Josephson junctions in qubit loop can provide a finite coupling strength g .

Since the amplitude of ac current I_0 is given in terms of the current jump in Eq. (13), the coupling strength g depends on the current jump δ . The coupling constant can be rewritten as

$$\begin{aligned} \frac{g}{\hbar\omega_r^0} &= \frac{\alpha\Phi_0}{2\pi} \frac{\sqrt{\omega_r}}{\omega_r^0 \sqrt{Ll}} \frac{1}{\sqrt{\frac{\hbar}{2\pi} \frac{\pi}{\sqrt{lcL}}}} \frac{\delta}{\sqrt{\frac{\hbar}{2\pi} \frac{\pi}{\sqrt{lcL}}}} \\ &= \frac{\alpha}{\pi} \frac{\Phi_0}{\sqrt{\hbar Z}} \sqrt{\frac{\omega_r}{\omega_r^0}} \frac{\delta}{\sqrt{2}}, \end{aligned} \quad (23)$$

where $\omega_r^0 = \pi/\sqrt{lcL}$ is the frequency of the 1st harmonic mode of the uniform resonator and $Z = \sqrt{l/c}$ is the impedance of the resonator [26]. In Fig. 4 we show the coupling constant g in the plane of $(d_0/d, w/w_0)$ for $Z = 50\Omega$ with $Ll = 2.5\text{nH}$ and $Lc = 1\text{pF}$ [7, 8], and thus $\Phi_0/\sqrt{\hbar Z} \approx 11.37$.

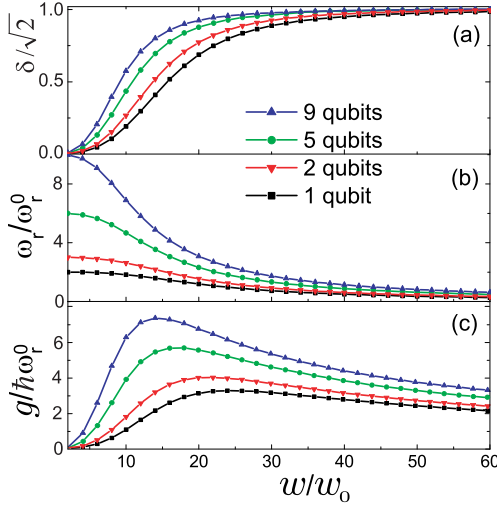


Fig. 5 (a) The current jump δ for $N = 1, 2, 5, 9$ qubits in the circuit of Fig. 1 as a function of w/w_0 along the diagonal line $w/w_0 = 2d_0/d$ in the bottom of Fig. 4. $\delta/\sqrt{2}$ increases along with w/w_0 and saturate to 1 finally. (b) The resonator frequency w_r decreases as w/w_0 increases. (c) The coupling constant g shows a maximum which is larger for more number of qubits.

In the case for more than one qubit in the circuit we calculate the coupling strength numerically. In Fig. 5 the behaviors of the current jump δ , the resonator frequency ω_r , and the coupling g along the diagonal line $w/w_0 = 2d_0/d$ in the plane of $(w/w_0, d_0/d)$ in Fig. 4 are shown. Large capacitance c' enables more charges to flow across the qubit, resulting in large ac current and thus large jump in Fig. 5(a). However the frequency of the resonator mode ω_r becomes small for large c' . The increase of w/w_0 and d_0/d makes the average capacitance of the resonator larger, and thus the resonator frequency $\omega_r \sim 1/\sqrt{c'}$ smaller [Fig. 5(b)]. As a result, the coupling g in Eq. (23) demonstrates a maximum because ω_r decreases while δ increases [Fig. 5(c)]. From Figs. 5 (b) and (c) it is shown that the ultrastrong coupling regime ($g \sim \hbar\omega_r$) is achievable with w and $1/d$ of just several multiples of w_0 and $1/d_0$. If there is one qubit in the circuit, the coupling shows a maximum where the coupling $g \sim 3\hbar\omega_r^0$ reaches deep strong coupling regime ($g > \hbar\omega_r$) [19,21,27].

If there are N qubits in the circuit, we can perform similar calculations numerically. For N qubits we need $(N+1)$ th harmonic mode in the resonator, and thus ω_r has larger value for more number of qubits [Fig. 5(b)]. Higher modes have a shorter wave length, and thus larger amount of ac current flows from the capacitance line of width w to the qubit. Indeed, the current jump δ becomes larger for more number of qubits [Fig. 5(a)]. As a result, the coupling g in Eq. (23) increases along with the number of qubits N [Fig. 5(c)]. Actually we have calculated the maximum coupling strength for $N = 1, 3, 5, 7, 9$ and found that the increasing rate slightly decreases. In the present scheme the dc-SQUIDS switch on just two qubits for qubit-qubit interaction, keeping other qubits switched off. Since only two qubits are coupled in the design, the collected decoherence rate will be not so much different from that of independent qubit.

There are some disadvantages in our scheme. Actually, we use a higher resonator mode in the design containing many qubits as shown in Fig. 1. However, it is known that the higher modes of the resonator have low quality factor which is proportional to $1/N$ for N -th mode [28]. In the present study we consider only one mode, namely $(N+1)$ -th mode for N qubits in one resonator. In order to be more accurate one should consider the multi mode effect. This effect is manifest, for example, in the studies of relaxation process of circuit-QED scheme by the Purcell effect [29] and of multi mode mediated qubit-qubit coupling [30,31]. A fuller treatment of the multi mode effect may be deferred to a future study.

In our scheme the flux qubit is coupled with the transmission line resonator through a capacitance. The structure of present current-biased flux qubit coupled with the ac current of resonator is very similar to the usual current-biased dc-SQUID qubit (phase qubit) [32]. The only difference is the number of Josephson junctions in the qubit loop, that is, the present qubit has three Josephson junctions and the phase qubit one or two junctions. In the present scheme the capacitance is introduced in order to couple the qubit with external current, and thus the main decoherence may come from the dephasing due to the noise of current flowing through the capacitance.

The current noise-induced dephasing of the phase qubit is given by $\langle \phi^2 \rangle \sim (S_q^*(1\text{Hz})/C)/\Delta U$ [33], where $S_q^*(1\text{Hz})$ is the noise spectral density, C the junction capacitance, and ΔU the barrier height of tilted potential. Since the noise spectral density scales as the junction area which is proportional to the junction capacitance, $S_q^*(1\text{Hz})/C$ is independent of the junction size [33]. Thus we can compare the dephasing rates of the present qubit and the phase qubit by estimating the barrier height of potential, ΔU . The barrier height of the phase qubit is given by $\Delta U = (2\sqrt{2}I_0\Phi_0/3\pi)(1 - I/I_0)^{3/2} \approx 2E_J(1 - I/I_0)^{3/2}$ with the Josephson coupling energy $E_J = I_0\Phi_0/2\pi$, the junction critical current I_0 , and the junction bias current I [33]. Since the junction bias current is typically driven close to the critical current such as $(1 - I/I_0) \sim 10^{-2}$ [32], the barrier height becomes very small, $\Delta U \approx 0.002E_J$, which results in the severe dephasing $\langle \phi^2 \rangle$ in the phase qubit. However, for our flux qubit we need not the dc-bias current I and thus $\Delta U'$ in the double well potential of qubit is very large compared to the phase qubit. For typical flux qubit with smaller junction of $E'_{J1}/E'_{J2} \approx 0.8$ we have $\Delta U' \sim 0.2E'_{J2}$ and the ratio of Josephson coupling energy of typical flux qubit to that of the phase qubit is $E'_{J2}/E_J \sim 0.1$. Hence the barrier height of present qubit $\Delta U'/\Delta U \sim 10$, which results in small dephasing rate compared to the phase qubit.

4 Two-qubit coupling

Single qubit gates can be performed by applying an external driving mode $\mathcal{H}_D = \epsilon a^\dagger e^{-i\omega_d t} + \epsilon^* a e^{i\omega_d t}$. The total Hamiltonian is written as $\mathcal{H}_t = \mathcal{H}_{\text{JC}} + \mathcal{H}_D$, where \mathcal{H}_{JC} is a Jaynes-Cummings type Hamiltonian in the rotating wave approximation (RWA) of \mathcal{H} in Eq. (21) [34]. By using the transformation $\mathcal{D}(\gamma) = e^{\gamma a^\dagger - \gamma^* a}$ with $\gamma(t) = -(\epsilon/\Delta_r)e^{-i\omega_d t}$ and $\Delta_r = \omega_r - \omega_d$, we can get the transformed Hamiltonian $\tilde{\mathcal{H}} = \mathcal{D}^\dagger \mathcal{H}_t \mathcal{D} - i\mathcal{D}^\dagger \dot{\mathcal{D}}$ given by

$$\tilde{\mathcal{H}} = \Delta_r a^\dagger a + \frac{\Delta_a}{2} \sigma_z - ig(a^\dagger \sigma_- - a \sigma_+) + \frac{\Omega_R}{2} \sigma_y \quad (24)$$

with $\Delta_a = \omega_a - \omega_d$. In the dispersive regime $|\Delta| \gg g$ with $\Delta = \omega_a - \omega_r$, the coupling between qubit and resonator can be eliminated by introducing the transformation $\mathcal{H}^* = \mathcal{U}^\dagger \tilde{\mathcal{H}} \mathcal{U}$ with $\mathcal{U} = e^{-i\frac{g}{\Delta}(a^\dagger \sigma_- + a \sigma_+)}$, resulting in $\mathcal{H}^* \approx \Delta_r a^\dagger a + \frac{\Delta_a}{2} \sigma_z + \chi(a^\dagger a + \frac{1}{2})\sigma_z + \frac{\Omega_R}{2} \sigma_y$ with the ac-Stark shift $\chi = g^2/\Delta$.

The universal gate in quantum computing requires a two-qubit gate in addition to the single qubit operation. In the scalable design of Fig. 1(a) the two-qubit Hamiltonian is given by

$$H_{2\text{qubit}} = \omega_r a^\dagger a + \sum_{j=1,2} \frac{\omega_{aj}}{2} \sigma_{zj} - i \sum_{j=1,2} g_j (a^\dagger \sigma_{-j} - a \sigma_{+j}) \quad (25)$$

in the rotating wave approximation for weak coupling strength $g_j/\omega_{aj} \ll 1$ [34].

The two-qubit Hamiltonian of Eq. (25) can be represented as $H_{2\text{qubit}} = H_{\text{cavity}} \otimes H_{\text{qubit1}} \otimes H_{\text{qubit2}}$ and we introduce a transformation matrix

$$U_2 = e^{-i\frac{\varphi_1}{\sqrt{2}}(a^\dagger\sigma_{-1}+a\sigma_{+1})-i\frac{\varphi_2}{\sqrt{2}}(a^\dagger\sigma_{-2}+a\sigma_{+2})} \quad (26)$$

in the same basis. Then the Hamiltonian $H_{2\text{qubit}}$ and the transformation matrix U_2 can be written in a block-diagonal form by slightly changing the order of basis. For simplicity, we consider nominally identical qubits, $\omega_{a1} = \omega_{a2} = \omega_a$, $g_1 = g_2 = g$, and thus $\varphi_1 = \varphi_2 = \varphi$, and then the lowest block involving the resonator photon number $n = 0$ and 1 in the Hamiltonian is represented in the basis $\{|1 \downarrow\downarrow\rangle, |0 \uparrow\downarrow\rangle, |0 \downarrow\uparrow\rangle\}$. Here $|\uparrow\rangle$ and $|\downarrow\rangle$ are the qubit states, and $|0\rangle$ and $|1\rangle$ are the photon number states.

Then we can easily check that if the condition $\tan 2\varphi = 2\sqrt{2}g/\Delta$ is satisfied, the transformed Hamiltonian $\tilde{H}_{2\text{qubit}} = U_2^\dagger H_{2\text{qubit}} U_2$ becomes block-diagonalized further, and describes the xy-type coupling between two states, $|0 \uparrow\downarrow\rangle$ and $|0 \downarrow\uparrow\rangle$, with the coupling constant

$$J = \frac{g}{\sqrt{2}} \tan \varphi. \quad (27)$$

J can be explicitly evaluated with above condition to provide the interaction Hamiltonian

$$H_{\text{int}} = \pm \frac{g^2}{\sqrt{\left(\frac{\Delta}{2}\right)^2 + 2g^2 + \frac{|\Delta|}{2}}} (\sigma_{-1}\sigma_{+2} + \sigma_{+1}\sigma_{-2}), \quad (28)$$

where the sign is $+$ for $\Delta > 0$ and $-$ for $\Delta < 0$ because $g > 0$. In the circuit-QED architecture the interaction between the resonator mode and the qubit can be discussed separately in the on-resonance regime ($|\Delta| = |\omega_a - \omega_r| \approx 0$) and the dispersive regime ($g/|\Delta| \ll 1$) [35]. This expression holds for the on-resonance regime as well as for the dispersive regime. In the on-resonance regime the interaction term becomes $H_{\text{int}} \approx \pm(g/\sqrt{2})(\sigma_{-1}\sigma_{+2} + \sigma_{+1}\sigma_{-2})$.

In real experiments, however, the two flux qubits may not be identical because of the different Josephson junction energies between two qubits. Then the qubit frequencies ω_{aj} with $j = 1, 2$ as well as the phase difference α_j 's across the small Josephson junction are different from each other. Further, the capacitance density c' around each qubit may also be different. As shown in Fig. 3 the current jump δ depends on the capacitance density c' . As a result, the qubit-resonator coupling strength g_j in Eq. (23) are also different from each other.

For this general case we can obtain the two-qubit interacting Hamiltonian in the dispersive regime. Since the condition $\tan 2\varphi = 2\sqrt{2}g/\Delta$ can be reduced to $\varphi \approx \sqrt{2}g/\Delta$ in the dispersive regime $|\Delta_j| = |\omega_{aj} - \omega_r| \gg g_j$, the transformation in Eq. (26) is approximately given by

$$U_2 = e^{-i\frac{g_1}{\Delta_1}(a^\dagger\sigma_{-1}+a\sigma_{+1})-i\frac{g_2}{\Delta_2}(a^\dagger\sigma_{-2}+a\sigma_{+2})}. \quad (29)$$

Then we can obtain the transformed Hamiltonian $\tilde{H}_{2\text{qubit}} = U_2^\dagger H_{2\text{qubit}} U_2$, resulting in

$$H_{\text{int}} = \frac{1}{2} \left(\frac{1}{\Delta_1} + \frac{1}{\Delta_2} \right) g_1 g_2 (\sigma_{-1} \sigma_{+2} + \sigma_{+1} \sigma_{-2}) \quad (30)$$

which can also be seen in the Hamiltonian for circuit-QED with superconducting charge qubits [2]. In the dispersive limit we can check that the Hamiltonian in Eq. (28) can be reduced to that in Eq. (30) for identical two qubits with $\Delta_1 = \Delta_2$ and $g_1 = g_2$.

5 Summary

In summary, we proposed a circuit QED architecture with superconducting flux qubits. The three-junctions flux qubit is coupled with the resonator by an ac current flowing through the capacitance between the qubit and the resonator. We introduced a scalable design with superconducting flux qubits, where the capacitance line extended from the qubit loop takes the role of leading the oscillating current into the qubit loop. As the capacitance between qubit and resonator increases, larger current flows through the qubit while the resonator mode frequency decreases. As a result, the qubit-resonator coupling shows a maximum of ultrastrong coupling with reasonable parameter values. The qubit-resonator coupling increases along with the number of qubits because a higher harmonic mode should be adopted. Two-qubit xy-type interaction can also be obtained from a scalable design for circuit QED architecture.

Acknowledgements The author acknowledges the useful discussion with K. Moon. This work was partly supported by Basic Science Research Program through the National Research Foundation of Korea (NRF) funded by the Ministry of Education, Science and Technology (2011-0023467) and by the IT R&D program of MOTIE/KEIT [10043464(2012)].

Conflict of Interest: The author declares that he has no conflict of interest.

References

1. A. Blais, R.-S. Huang, A. Wallraff, S. M. Girvin, and R. J. Schoelkopf, Cavity quantum electrodynamics for superconducting electric circuits: An architecture for quantum computation, *Phys. Rev. A* **69**, 062320 (2004).
2. A. Blais, J. Gambetta, A. Wallraff, D. I. Schuster, S. M. Girvin, M. H. Devoret, and R. J. Schoelkopf, Quantum-information processing with circuit quantum electrodynamics, *Phys. Rev. A* **75**, 032329 (2007).
3. J. E. Mooij, T. P. Orlando, L. Levitov, L. Tian, C. H. van der Wal, and S. Lloyd, Josephson persistent-current qubit, *Science* **285**, 1036 (1999); I. Chiorescu, Y. Nakamura, C. J. P. M. Harmans, and J. E. Mooij, Coherent quantum dynamics of a superconducting flux qubit, *Science* **299**, 1869 (2003).
4. T. P. Orlando, J. E. Mooij, L. Tian, C. H. van der Wal, L. S. Levitov, Seth Lloyd, and J. J. Mazo, Superconducting persistent-current qubit, *Phys. Rev. B* **60**, 15398 (1999).
5. M. D. Kim, D. Shin, and J. Hong, Double-well potentials in current qubits, *Phys. Rev. B* **68**, 134513 (2003).

6. T. Lindstrom, C. H. Webster, J. E. Healey, M. S. Colclough, C. M. Muirhead, and A. Y. Tzalenchuk, Circuit QED with a flux qubit strongly coupled to a coplanar transmission line resonator, *Supercond. Sci. Technol.* **20**, 814 (2007).
7. G. Oelsner, S. H. W. van der Ploeg, P. Macha, U. Hubner, D. Born, S. Anders, E. Il'ichev, H.-G. Meyer, M. Grajcar, S. Wünsch and M. Siegel, A. N. Omelyanchouk, and O. Astafiev, Weak continuous monitoring of a flux qubit using coplanar waveguide resonator, *Phys. Rev. B* **81**, 172505 (2010).
8. A. A. Abdumalikov, Jr., O. Astafiev, Y. Nakamura, Y. A. Pashkin, and J. S. Tsai, *Phys. Rev. B* **78**, 180502(R) (2008); J. Bourassa, J. M. Gambetta, A. A. Abdumalikov, Jr., O. Astafiev, Y. Nakamura, and A. Blais, Ultrastrong coupling regime of cavity QED with phase-biased flux qubits, *Phys. Rev. A* **80**, 032109 (2009).
9. T. Niemczyk, F. Deppe, H. Huebl, E. P. Menzel, F. Hocke, M. J. Schwarz, J. J. Garcia-Ripoll, D. Zueco, T. Hummer, E. Solano, A. Marx, and R. Gross, Circuit quantum electrodynamics in the ultrastrong-coupling regime, *Nature Phys.* **6**, 772 (2010).
10. P. Forn-Diaz, J. Lisenfeld, D. Marcos, J. J. Garcia-Ripoll, E. Solano, C. J. P. M. Harms, and J. E. Mooij, Observation of the Bloch-Siegert shift in a qubit-oscillator system in the ultrastrong coupling regime, *Phys. Rev. Lett.* **105**, 237001 (2010).
11. M. D. Kim and K. Moon, Strong coupling of a cavity QED architecture for a current-biased flux qubit, *J. Korean Phys. Soc.* **58**, 1599 (2011); arXiv: 1005.1703.
12. M. Steffen, S. Kumar, D. P. DiVincenzo, J. R. Rozen, G. A. Keefe, M. B. Rothwell, and M. B. Ketchen, High-coherence hybrid superconducting qubit, *Phys. Rev. Lett.* **105**, 100502 (2010).
13. J. M. Chow, A. D. Corcoles, J. M. Gambetta, C. Rigetti, B. R. Johnson, J. A. Smolin, J. R. Rozen, G. A. Keefe, M. B. Rothwell, M. B. Ketchen, and M. Steffen, Simple all-microwave entangling gate for fixed-frequency superconducting qubits, *Phys. Rev. Lett.* **107**, 080502 (2011).
14. K. Inomata, T. Yamamoto, P.-M. Billangeon, Y. Nakamura, and J. S. Tsai, Large dispersive shift of cavity resonance induced by a superconducting flux qubit in the straddling regime, *Phys. Rev. B* **86**, 140508(R) (2012).
15. J. M. Martinis, S. Nam, J. Aumentado, and C. Urbina, Rabi oscillations in a large Josephson-junction qubit, *Phys. Rev. Lett.* **89**, 117901 (2002).
16. J. M. Martinis, Superconducting phase qubits, *Quantum Inf. Process.* **8**, 81 (2009).
17. A. J. Berkley, H. Xu, R. C. Ramos, M. A. Gubrud, F. W. Strauch, P. R. Johnson, J. R. Anderson, A. J. Dragt, C. J. Lobb, and F. C. Wellstood, Entangled macroscopic quantum states in two superconducting qubits, *Science* **300**, 1548 (2003).
18. M. A. Sillanpää, J. I. Park, and R. W. Simmonds, Coherent quantum state storage and transfer between two phase qubits via a resonant cavity, *Nature* **449**, 438 (2007).
19. D. Ballester, G. Romero, J. J. Garcia-Ripoll, F. Deppe, and E. Solano, Quantum simulation of the ultrastrong-coupling dynamics in circuit quantum electrodynamics, *Phys. Rev. X* **2**, 021007 (2012).
20. P. Nataf and C. Ciuti, Protected quantum computation with multiple resonators in ultrastrong coupling circuit QED, *Phys. Rev. Lett.* **107**, 190402 (2011)
21. G. Romero, D. Ballester, Y. M. Wang, V. Scarani, and E. Solano, Ultrafast quantum gates in circuit QED, *Phys. Rev. Lett.* **108**, 120501 (2012).
22. J. Majer, J. M. Chow, J. M. Gambetta, J. Koch, B. R. Johnson, J. A. Schreier, L. Frunzio, D. I. Schuster, A. A. Houck, A. Wallraff, A. Blais, M. H. Devoret, S. M. Girvin, and R. J. Schoelkopf, Coupling superconducting qubits via a cavity bus, *Nature* **449**, 443 (2007).
23. See, e.g., J. Q. You, Y. Nakamura, and F. Nori, Fast two-qubit operation in inductively coupled qubits, *Phys. Rev. B* **71**, 024532 (2005).
24. J. Q. You, X. Hu, S. Ashhab, and F. Nori, Low-decoherence flux qubit, *Phys. Rev. B* **75**, 140515(R) (2007).
25. See, e.g., M. Tinkham, *Introduction to superconductivity* (McGraw Hill, New York, ed. 2, 1996).
26. R.-S. Huang, Qubit-resonator system as an application to quantum computation, PhD thesis, Indiana Univ. (2004).
27. J. Casanova, G. Romero, I. Lizuain, J. J. García-Ripoll, and E. Solano, Deep strong coupling regime of the Jaynes-Cummings model, *Phys. Rev. Lett.* **105**, 263603 (2010).

28. M. Göppl, A. Fragner, M. Baur, R. Bianchetti, S. Filipp, J. M. Fink, P. J. Leek, G. Puebla, L. Steffen, and A. Wallraff, Coplanar waveguide resonators for circuit quantum electrodynamics, *J. Appl. Phys.* **104**, 113904 (2008).
29. A. A. Houck, J. A. Schreier, B. R. Johnson, J. M. Chow, J. Koch, J. M. Gambetta, D. I. Schuster, L. Frunzio, M. H. Devoret, S. M. Girvin, and R. J. Schoelkopf, Controlling the Spontaneous Emission of a Superconducting Transmon Qubit, *Phys. Rev. Lett.* **101**, 080502 (2008).
30. S. Filipp, M. Göppl, J. M. Fink, M. Baur, R. Bianchetti, L. Steffen, and A. Wallraff, Multimode mediated qubit-qubit coupling and dark-state symmetries in circuit quantum electrodynamics, *Phys. Rev A* **83**, 063827 (2011).
31. D. C. McKay, R. Naik, P. Reinhold, L. S. Bishop, and D. I. Schuster, High-Contrast Qubit Interactions Using Multimode Cavity QED, *Phys. Rev. Lett.* **114**, 080501 (2015).
32. R.W. Simmonds, K.M. Lang, D. A. Hite, S. Nam, D. P. Pappas, and J. M. Martinis, Decoherence in Josephson Phase Qubits from Junction Resonators, *Phys. Rev. Lett.* **93**, 077003 (2004).
33. J. M. Martinis, S. Nam, J. Aumentado, and K. M. Lang, Decoherence of a superconducting qubit due to bias noise, *Phys. Rev. B* **67**, 094510 (2003).
34. E. T. Jaynes and F. W. Cummings, Comparison of quantum and semiclassical radiation theories with application to the beam maser, *Proc. IEEE* **51**, 89 (1963).
35. A. Wallraff, D. I. Schuster, A. Blais, L. Frunzio, R.-S. Huang, J. Majer, S. Kumar, S. M. Girvin and R. J. Schoelkopf, Strong coupling of a single photon to a superconducting qubit using circuit quantum electrodynamics, *Nature* **431**, 162 (2004).